The role of growth temperature on the indium incorporation process for the MOCVD growth of InGaN/GaN heterostructures

Sauffi Bin Yusof, Zainuriah Hassan, Sidi Ould Saad Hamady, Sha Shiong Ng, Mohd Anas Ahmad, Way Foong Lim, Muhd Azi Che Seliman, Christyves Chevallier, Nicolas Fressengeas

▶ **To cite this version:**

Sauffi Bin Yusof, Zainuriah Hassan, Sidi Ould Saad Hamady, Sha Shiong Ng, Mohd Anas Ahmad, et al.. The role of growth temperature on the indium incorporation process for the MOCVD growth of InGaN/GaN heterostructures. Microelectronics International, 2021, 38 (3), pp.105-112. 10.1108/MI-02-2021-0018 . hal-03247074

HAL Id: hal-03247074

https://hal.univ-lorraine.fr/hal-03247074

Submitted on 12 Feb 2022

HAL is a multi-disciplinary open access archive for the deposit and dissemination of scientific research documents, whether they are published or not. The documents may come from teaching and research institutions in France or abroad, or from public or private research centers.

L'archive ouverte pluridisciplinaire **HAL**, est destinée au dépôt et à la diffusion de documents scientifiques de niveau recherche, publiés ou non, émanant des établissements d'enseignement et de recherche français ou étrangers, des laboratoires publics ou privés.

Ahmad Sauffi Yusof (1,2), Zainuriah Hassan (2), Sidi Ould Saad Hamady (1), Sha Shiong Ng (2), Mohd Anas Ahmad (2), Way Foong Lim (2), Muhd Azi Che Seliman (2), Christyves Chevallier (1) and Nicolas Fressengeas (1)

(1) Institute of Nano Optoelectronics Research and Technology (INOR), Universiti Sains Malaysia, Penang, Malaysia
(2) Laboratoire Matériaux Optiques, Photonique et Systèmes (LMOPS), CentraleSupélec, Université de Lorraine, Metz,

The role of growth temperature on the indium incorporation process for the MOCVD growth of InGaN/GaN heterostructures

Abstract

Purpose – The purpose of this paper is to investigate the effect of growth temperature on the evolution of indium incorporation and the growth process of InGaN/GaN heterostructures.

Design/methodology/approach – To examine this effect, the InGaN/GaN heterostructures were grown using Taiyo Nippon Sanso Corporation (TNSC) metal-organic chemical vapor deposition (MOCVD) SR4000-HT system. The InGaN/GaN heterostructures were epitaxially grown on 3.4 μm undoped-GaN (ud-GaN) and GaN nucleation layer, respectively, over a commercial 2" c-plane flat sapphire substrate (FSS). The InGaN layers were grown at different temperature settings ranging from 860°C to 820°C in a step of 20°C. The details of structural, surface morphology and optical properties were investigated using X-ray diffraction (XRD), field emission scanning electron microscope (FE-SEM), atomic force microscopy (AFM) and ultraviolet-visible (UV-Vis) spectrophotometer, respectively.

Findings – InGaN/GaN heterostructure with indium composition up to 10.9% has been successfully grown using the MOCVD technique without any phase separation detected within the sensitivity of the instrument. Indium compositions were estimated through simulation fitting of the XRD curve and calculation of Vegard's law from UV-Vis measurement. The thickness of the structures was determined using the Swanepoel method and the FE-SEM cross-section image.

Originality/value – This paper report on the effect of MOCVD growth temperature on the growth process of InGaN/GaN heterostructure, which is of interest in solid-state lighting technology, especially in light-emitting diodes (LEDs) and solar cells application.

Keywords II-nitride semiconductor, InGaN, MOCVD

Paper type Research paper

1. Introduction

The nitride-based semiconductor system, which includes GaN, AlN, InN, and its related alloys, has been extensively developed due to its wide range of practical applications, especially in optoelectronic and power devices (Moustakas and Paiella, 2017; Shur, 2019). Since the InN possesses a narrow bandgap value at 0.64 eV, the fundamental bandgap of III-V alloy materials such as InGaN can be extended into a broader range of the spectral region (Walukiewicz *et al.*, 2006). In recent years, the III-V nitride materials system has shown its capability where high-efficiency light-emitting diodes (LEDs) have been reported using InGaN-based ternary alloy as the active materials (Jiang *et al.*, 2015; Iida *et al.*, 2020). This sparked immense scientific interest in this area to develop high-efficiency InGaN-based solar cells compared to conventional silicon or cadmium telluride structures (Ould Saad Hamady, Adaine and Fressengeas, 2016; Valdueza-Felip *et al.*, 2017).

The interest came from its intrinsic properties such as tuneable wide bandgap, high absorption coefficient (10^5 cm^{-1}), and high thermal stability (Jani *et al.*, 2007; Lu and Ferguson, 2013). The bandgap energies of InGaN ternary alloy can be engineered from 0.64 eV to 3.4 eV solely by changing the indium composition in the structure. InGaN also has strong interatomic bonds and high thermal conductivity, giving the photovoltaic solar panel an advantage to become more resistive to high energy radiation and operate in harsh environments (Adaine, Hamady and Fressengeas, 2017). Thus, making InGaN an outstanding candidate for high-efficiency full solar spectrum photovoltaic cell devices. The theoretical external and internal energy conversion efficiency of InGaN-based solar cells can be achieved up to 43% and 60%, respectively, making it is superior to silicon and chalcogenide-based solar cells (Zeng *et al.*, 2009).

From a practical standpoint, however, the photovoltaic performance of GaN/InGaN heterojunction and InGaN homojunction has been demonstrated previously with relatively low efficiency and poor performance (Bhuiyan *et al.*, 2012). Despite the rapid development for the past few years of these materials in LEDs technology (as active materials) (Baek, Lee and Lee, 2019), the main bottleneck that would limit its photovoltaic performance arose from the difficulty in growing high-quality In-rich InGaN films (Wolny *et al.*, 2018). This problem was attributed to the intrinsic properties of the binary InN and GaN. The large difference in the interatomic spacing of InN compared to GaN would result in a solid phase miscibility gap within the grown structure (Yamamoto *et al.*, 2013). At a specific range of the InGaN alloy mixture, the thermodynamically unstable InGaN phase will undergo spontaneous spinodal decomposition into multiple thermodynamically stable phases, which will induce phase separation and composition inhomogeneity within the grown structure.

Furthermore, the relatively low vapor pressure of GaN compared to InN can results in low absorption of indium in the InGaN structure during the growth process. In addition, the difference in the enthalpy formation of binary InN and GaN can lead to strong indium segregation in the growth front (Guo *et al.*, 2010; Kadys *et al.*, 2015). However, few approaches have been reported to minimize the problems, mainly by optimizing the growth parameters such as relatively low growth temperature, high V/III ratio,

low growth rate, and low growth pressure (Yam and Hassan, 2008). In this work, InGaN/GaN heterostructures were epitaxially grown using MOCVD techniques on a flat and patterned sapphire substrate. The effect of buffer layer thickness on the optoelectronic properties and crystallinity defect, as well as the correlation with its physical properties, were investigated.

2. Experimental details

The InGaN structures were epitaxially grown on ~3.4 μm thick undoped-GaN (ud-GaN) and low-temperature GaN buffer layer (LTBL) over a commercial 2" c-plane flat sapphire substrate (FSS) using the Taiyo Nippon Sanso Corporation (TNSC) metal-organic chemical vapor deposition (MOCVD) SR4000-HT system with horizontal reactor configuration. Prior to the epitaxial growth, the substrates were thermally clean under H_2 ambient at elevated temperature to remove any impurities and native oxide on the surface of the substrates. The structure is comprised of a LTBL layer, ud-GaN layer, and InGaN layer. The schematic representation cross-sectional view of the grown structures is shown in Fig. 1. Then, the temperature was reduced to 200 °C before opening the reactor.

Trimethylgallium (TMGa) and ammonia (NH_3) were used as gallium and nitrogen precursors, respectively, with H_2 as the carrier gas for ud-GaN and GaN nucleation layers at a V/III ratio of 3800 and 3044, respectively. For the InGaN layer, triethylgallium (TEGa), trimethylindium (TMIn) and NH_3 were used as gallium, indium and nitrogen precursors, respectively, with N_2 as the carrier gas. The V/III and TMIn/III ratios were fixed at 15177 and 57.2%, respectively. The growth temperature settings for the InGaN layer were varied from 860 °C to 820 °C in a step of 20 °C. All other growth parameters were fixed. The InGaN layers growth conditions are summarized in Table I.

The crystallinity and phase identification of the grown structure were determined using high-resolution X-ray diffraction (HRXRD, Bruker D8 Discover) system with a triple-axis configuration on symmetric (0002). Simulation fitting of the XRD triple-axis curves was used to estimate the indium composition of the grown structure. The surface morphology and the structural changes of the grown structure were observed by using a field emission scanning electron microscope (FE-SEM, FEI Nova NanoSEM 450). Lastly, an ultraviolet-visible-near infrared (UV-Vis-NIR) spectrometer (Agilent Technology carry series) spectrometer was used to study the optical properties of the grown structure.

3. Results and discussion

Fig. 2 (a) shows the XRD ω-2θ curve patterns of InGaN/GaN heterostructures as a function of InGaN growth temperature. As shown in Fig. 2 (a), all structure possesses two sharp diffraction peaks at ω-2θ = 34.57° and ω-2θ = 33.97°, 34.23°, and 34.35° which correspond to GaN and InGaN layers, respectively. The indium composition as well as the thickness of the InGaN layer can be estimated through the simulation fitting of ω-2θ scan on (0002) plane as shown in Fig. 2 (a) and summarized in Fig. 2 (b) and Table II. The shift in XRD InGaN peaks to a lower angle as a function of the InGaN growth temperature is due to the different amounts of indium that has been successfully incorporated into the structure during the growth process.

From the simulation fitting value, the indium incorporations were increased with the decrease in the growth temperature, similarly reported in previous literature (Tao *et al.*, 2011; Surender *et al.*, 2017). It is well known that the growth of the InGaN epilayer is not a straightforward process due to the high saturation of InN vapor pressure. Thus, by lowering the growth temperature, it will reduce the probability of indium to be desorb at the growth front and subsequently increase the rate of the indium to be incorporated into the grown structure. Furthermore, the reduction in the intensity of InGaN ω-2θ peaks can be observed as a function of InGaN growth temperature, indicating the decline in the overall quality of the InGaN layer. It is well-known that the MOCVD growth process depends heavily on the growth temperature and the flow rate of the precursor that flow into the reactor (Oliver *et al.*, 2005; Durkaya *et al.*, 2010; Howlader *et al.*, 2014).

The growth temperature can dictate the stability of the precursor and influence the outcome of the grown structure. For example, when the growth process was carried out at relatively low temperatures or known as the kinetically limited region, the cracking of NH_3 will become inefficient and reduce the quality of the grown structure (Cavalcoli, Plaickner and Vogt, 2013; Tassev and Vangala, 2019). In contrast, when the growth process was carried out at a relatively high temperature or known as thermodynamically limited region, the desorption of indium will become dominant, reducing the probability for the indium to be incorporated into the grown structure (Bosi and Fornari, 2004; X. Wang *et al.*, 2018).

The InGaN growth temperature effects on the surface morphology of the InGaN/GaN heterostructures were studied using FE-SEM measurement, as shown in Fig. 3 and Fig. 4. From the observation, all samples showing the presence of V-pits on the surface of the structure similarly reported in previous literature (Bag *et al.*, 2018). The surface pits density and size were increased with the decrease in the InGaN growth temperature. When the growth process was carried out at a relatively low temperature, the mobility of adatoms on the growing surface will be reduced (Son *et al.*, 2004). These can cause a high incident point defect and structural instability within the grown structure, leading to a structural defect such as V-pits (Smalc-Koziorowska *et al.*, 2015). No indium droplets were observed within the FE-SEM scan area (surface and cross-section image). The overall thickness of InGaN/GaN heterostructure with InGaN layer grown at 860 °C is estimated at 3870 nm from the FE-SEM cross-section image as shown in Fig. 4.

Fig. 5 (a) shows the typical transmittance curve of InGaN/GaN heterostructure as a function of InGaN growth temperature at the range from 300 nm to 2500 nm obtained from the UV-Vis-NIR spectrometer measurement. As observed in Fig. 5 (a), a strong modulation pattern is found in the transmittance curve caused by the difference in the refractive index of the grown structure at sapphire/GaN and InGaN/Air interface. This phenomenon is called Fabry-Perot etalon effect (Hums *et al.*, 2007). Thus, to clearly observed the graphical representation of the transmittance curve within each sample, the graph of transmittance enveloped mean was plotted as shown in Fig. 5

(c) by using the following expression (Márquez *et al.*, 1992): -

$$T_\alpha = (T_M \times T_m)^{\frac{1}{2}} \tag{1}$$

where T_α, T_M and T_m are transmittance envelope geometric means, transmittance upper envelope and transmittance lower envelope respectively, as shown in Fig. 5 (b).

All samples possess high transmittance at above 80% in the visible region that extends into the infrared region. The spike of the transmittance spectra at ~830 nm is from the instrument feature. The lamps of the spectrometer do not properly align mechanically during the instrument switching its light source. All structures showed a sharp absorption cut-off at ~366 nm, which was caused by the GaN layer. When the InGaN growth temperature was reduced to 820 °C, it will induce a broad absorption of light in the visible region, similarly reported in previous literature (Yusof *et al.*, 2021), which is caused by the smaller bandgap of the InGaN layer. The improvement in overall transmittance of the grown structure in the visible region that extended into the infrared region is observed when the InGaN layer was grown at 840 °C. However, additional measurement and proof would be needed to explain this behavior since the optical transmittance is also affected by surface scattering and impurity absorption (H. L. Wang *et al.*, 2018).

From the transmittance spectra, the optical bandgap of the grown structure can be calculated by using the following Tauc expression (Jakkala and Kordesch, 2017): -

$$(ahv)^2 = A\left(hv - E_g\right)^n \tag{2}$$

where a, hv, A, E_g, and n are absorption coefficient, Planck's equation (photon energy), a constant value that depends on transition probability, optical energy gap, and a value that depend on the nature transition of electron (direct allowed semiconductor; $n = 1/2$), respectively. The absorption coefficient of the structure can be calculated by using the following Beer-Lambert law relation (Yusof, Hassan and Zainal, 2018): -

$$I_e = I_i e^{-ad} \tag{3}$$

$$T = \frac{I_e}{I_i} \tag{4}$$

where T, I_i, I_e, a, and d are transmittance, incident light, transmitted light, absorption coefficient, and thickness of the structure, respectively. Then, by extrapolating the straight line in the graph of $(\alpha hv)^2$ as a function of photon energy (hv) to the point of x-intercept at $(\alpha hv)^2 = 0$, the optical energy gap of the grown structure can be determined as shown in Fig. 6.

As observed, there are two well-distinguished energy states at E_g = 3.39 eV and E_g = 3.26 eV, 3.16 eV, 2.96 eV, which belong to GaN and InGaN layer, respectively. The optical band of the GaN layer (3.39 eV) obtained from this method is in good agreement with previous literature (Tsao *et al.*, 2018). Since the change in the band gap of InGaN layers are in correlation with the indium composition within the grown InGaN layer, Vegard's law can be implemented to calculate the indium composition through the following relation (Yam and Hassan, 2008): -

$$E_g(In_xGa_{1-x}N) = xE_g(InN) + (1-x)E_g(GaN) - bx(1-x) \tag{5}$$

where b is the bowing parameter. The precise value of the InGaN ternary alloy bowing parameter has long been a subject of debate. A recent study on band bowing in InGaN alloy shows that the bowing parameter's value strongly depends on the indium composition (Moses *et al.*, 2011; Ohsawa, 2016). However, we used the universally agreed bowing parameter value from the previous literature at 1.4 eV for this calculation (Redaelli *et al.*, 2015; Wang *et al.*, 2016). Thus, this is probably the reason that the calculated indium composition value, especially at low indium composition, is slightly different from the value obtained at the simulation fitting of the XRD measurement. The calculated indium compositions were summarized in Table III.

Furthermore, as these strong modulation patterns were present in the transmittance spectra, the Swanepoel method can be used to calculate the overall thickness of the grown structure (Dı *et al.*, 2006; Shaaban and Yahia, 2012). The Swanepoel method is based on calculating the upper (T_M) and lower (T_m) bounding envelope curve as a function of transmittance spectra, which calculated by parabolic interpolation of the determined peaks and valleys in the modulation pattern of the transmittance spectra. Then, the refractive index (n) of the grown structure with respect to the transparent, medium and weak absorption region can be calculated by using the following expression: -

$$n = \left[N + (N^2 - s^2)^{\frac{1}{2}}\right]^{\frac{1}{2}} \tag{6}$$

where

$$N = \frac{s^2 + 1}{2} + \frac{2s}{T_m} \tag{7}$$

for visible regions

$$N = \frac{s^2 + 1}{2} + \frac{2s(T_M - T_m)}{T_M \times T_m} \quad (8)$$

and for weak and medium absorption regions. Where s is the refractive index of the substrate (Al_2O_3) as a function of wavelength, which was obtained from previous literature (Malitson, 1962). Following the Swanepoel method, the thickness of the grown structure (d) can be estimated using the calculated refractive index (n_1 and n_2) at adjacent maxima or minima value (λ_1 and λ_2) as a function of wavelength through the following expression: -

$$d_1 = \frac{M\lambda_1\lambda_2}{2(\lambda_2 n_1 - \lambda_1 n_2)} \quad (9)$$

where M relies on adjacent extreme type. M = 1 for two same adjacent extremes (maximum-maximum or minimum-minimum) and $M = 1/2$ for two adjacent opposite extremes (maximum-minimum or minimum-maximum). By using the basic equation of the interference fringes, the new order number (m_o) can be calculated: -

$$2nd = m_o\lambda \quad (10)$$

where m_o could be assumed to be $m_o = 1$ or 1/2, depending on extreme type; maximum or minimum, respectively. Then, by knowing the exact integer or half-integer value of the order number associated with each extreme, a new thickness with higher precision and lower dispersion can be derived, which were then summarized in Table IV.

The overall thickness of the grown structure estimated using the Swanepoel method showed slightly different from the thickness estimated from the FE-SEM cross-section image, as shown in Fig. 4. Since the Swanepoel method is heavily dependent on the modulation pattern in the transmittance spectra, the use of single-sided polished sapphire in this work could cause slight inaccuracy in the modulation measurement (Muth *et al.*, 1997). The light could be scattered at the unpolished side of the substrate during the spectrometer measurement, which can change the amplitude and position of the modulation pattern in the transmittance spectra.

4. Summary and conclusion

InGaN/GaN heterostructure with indium composition up to 10.9% has been successfully grown on FSS using the MOCVD technique. A well-resolved GaN and InGaN peaks at ω-2θ = 34.57° and ω-2θ = 33.97°, 34.23°, and 34.35° respectively without any additional peaks that correspond to composition inhomogeneities were obtained from the XRD measurement. The thickness and the indium composition of the grown structure were obtained through the simulation fitting of ω-2θ scan on (0002) plane. From the FE-SEM measurement, a surface-related defect such as V-pits can be observed on the surface of all the samples. The optical band gap and overall thickness of the samples were calculated using the Tauc plot and the Swanepoel method from the transmittance spectra. Secondary energy gap at E_g = 3.26 eV, 3.16 eV, 2.96 eV can be obtained from the Tauc plot, confirming the incorporation of indium into the grown structure. The indium composition and overall thickness of the grown structure obtained in this work were summarized in Table V.

References

Adaine, A., Hamady, S. O. S. and Fressengeas, N. (2017) 'Effects of structural defects and polarization charges in InGaN-based double-junction solar cell', *Superlattices and Microstructures*, Vol. 107, pp. 267–277. doi: 10.1016/j.spmi.2017.04.025.

Baek, S. H., Lee, H. J. and Lee, S. N. (2019) 'High-performance flat-type InGaN-based light-emitting diodes with local breakdown conductive channel', *Scientific Reports*, Vol. 9 No. 1, pp. 1–7. doi: 10.1038/s41598-019-49727-4.

Bag, A. *et al.* (2018) 'Evolution of lateral V-defects on InGaN/GaN on Si(111) during PAMBE: The role of strain on defect kinetics', *CrystEngComm*, Vol. 20 No. 29, pp. 4151–4163. doi: 10.1039/c8ce00577j.

Bhuiyan, A. G. *et al.* (2012) 'InGaN solar cells: Present state of the art and important challenges', *IEEE Journal of Photovoltaics*, Vol. 2 No. 3, pp. 276–293. doi: 10.1109/JPHOTOV.2012.2193384.

Bosi, M. and Fornari, R. (2004) 'A study of Indium incorporation efficiency in InGaN grown by MOVPE', *Journal of Crystal Growth*, Vol. 265 No. 3–4, pp. 434–439. doi: 10.1016/j.jcrysgro.2004.02.103.

Cavalcoli, D., Plaickner, J. and Vogt, P. (2013) 'Surface preparation and characterization of semipolar (20-21) InGaN layers', in. Available at: https://amslaurea.unibo.it/id/eprint/6643.

Dı, A. *et al.* (2006) 'Determination of optical properties in nanostructured thin films using the Swanepoel method', *Acta Physica Polonica A*, Vol. 252, pp. 6013–6017. doi: 10.1016/j.apsusc.2005.11.009.

Durkaya, G. *et al.* (2010) 'The influence of the group V/III molar precursor ratio on the structural properties of ingan layers grown by HPCVD', *Physica Status Solidi (A) Applications and Materials Science*, Vol. 207 No. 6, pp. 1379–1382. doi: 10.1002/pssa.200983622.

Guo, Y. *et al.* (2010) 'A study of indium incorporation in In-rich InGaN grown by MOVPE', *Applied Surface Science*, Vol. 256 No. 10, pp. 3352–3356. doi: 10.1016/j.apsusc.2009.11.081.

Howlader, M. A. H. *et al.* (2014) 'Analysis of phase separation in InGaN epitaxy for advanced solar cells', *Proceedings of 2014 3rd International Conference on the Developments in Renewable Energy Technology, ICDRET 2014*, pp. 4–8. doi:

10.1109/icdret.2014.6861728.
Hums, C. *et al.* (2007) 'Fabry-Perot effects in InGaN/GaN heterostructures on Si-substrate', *Journal of Applied Physics*, Vol. 101 No. 3, p. 33113. doi: 10.1063/1.2434010.
Iida, D. *et al.* (2020) 'Demonstration of low forward voltage InGaN-based red LEDs', *Applied Physics Express*, Vol. 13 No. 3, p. 31001. doi: 10.35848/1882-0786/ab7168.
Jakkala, P. and Kordesch, M. E. (2017) 'Bandgap tuning and spectroscopy analysis of Inx Ga(1-x) N thin films grown by RF sputtering method', *Materials Research Express*, Vol. 4 No. 1. doi: 10.1088/2053-1591/aa5111.
Jani, O. *et al.* (2007) 'Design and characterization of GaNInGaN solar cells', *Applied Physics Letters*, Vol. 91 No. 13, pp. 1–4. doi: 10.1063/1.2793180.
Jiang, Y. *et al.* (2015) 'Realization of high-luminous-efficiency InGaN light-emitting diodes in the "green gap" range', *Scientific Reports*, Vol. 5 No. May, pp. 1–7. doi: 10.1038/srep10883.
Kadys, A. *et al.* (2015) 'Growth of InN and In-Rich InGaN Layers on GaN Templates by Pulsed Metalorganic Chemical Vapor Deposition', *Journal of Electronic Materials*, Vol. 44. doi: 10.1007/s11664-014-3494-6.
Lu, N. and Ferguson, I. (2013) 'III-nitrides for energy production: photovoltaic and thermoelectric applications', *Semiconductor Science and Technology*, Vol. 28 No. 7, p. 74023. doi: 10.1088/0268-1242/28/7/074023.
Malitson, I. H. (1962) 'Refraction and Dispersion of Synthetic Sapphire', *Journal of the Optical Society of America*, Vol. 52 No. 12, p. 1377. doi: 10.1364/josa.52.001377.
Márquez, E. *et al.* (1992) 'Calculation of the thickness and optical constants of amorphous arsenic sulphide films from their transmission spectra', *Journal of Physics D: Applied Physics*, Vol. 25 No. 3, pp. 535–541. doi: 10.1088/0022-3727/25/3/031.
Moses, P. G. *et al.* (2011) 'Hybrid functional investigations of band gaps and band alignments for AlN, GaN, InN, and InGaN', *Journal of Chemical Physics*, Vol. 134 No. 8. doi: 10.1063/1.3548872.
Moustakas, T. D. and Paiella, R. (2017) 'Optoelectronic device physics and technology of nitride semiconductors from the UV to the terahertz', *Reports on Progress in Physics*, Vol. 80 No. 10, p. 106501. doi: 10.1088/1361-6633/aa7bb2.
Muth, J. F. *et al.* (1997) 'Absorption coefficient, energy gap, exciton binding energy, and recombination lifetime of GaN obtained from transmission measurements', *Applied Physics Letters*, Vol. 71 No. 18, pp. 2572–2574. doi: 10.1063/1.120191.
Ohsawa, J. (2016) 'Electrical characterization of metal–semiconductor–metal structure of pseudomorphic InGaN on GaN: Simulation and experiments', *Physica Status Solidi (A) Applications and Materials Science*, Vol. 213 No. 6, pp. 1602–1609. doi: 10.1002/pssa.201533047.
Oliver, R. A. *et al.* (2005) 'Growth modes in heteroepitaxy of InGaN on GaN', *Journal of Applied Physics*, Vol. 97 No. 1. doi: 10.1063/1.1823581.
Ould Saad Hamady, S., Adaine, A. and Fressengeas, N. (2016) 'Numerical simulation of InGaN Schottky solar cell', *Materials Science in Semiconductor Processing*, Vol. 41, pp. 219–225. doi: https://doi.org/10.1016/j.mssp.2015.09.001.
Redaelli, L. *et al.* (2015) 'Effect of the barrier thickness on the performance of multiple-quantum-well InGaN photovoltaic cells', *Japanese Journal of Applied Physics*, Vol. 54 No. 7, p. 72302. doi: 10.7567/jjap.54.072302.
Shaaban, E. R. and Yahia, I. S. (2012) 'Validity of Swanepoel ' s Method for Calculating the Optical Constants of Thick Films Optical constants , dispersion and oscillator parameters of di erent thicknesses of amorphous Ge 25 Cd 5 Se 70 have been investigated by optical spectrophotometry measur', *Applied Surface Science*, Vol. 121 No. 3, pp. 628–635.
Shur, M. (2019) 'Wide band gap semiconductor technology: State-of-the-art', *Solid-State Electronics*, Vol. 155, pp. 65–75. doi: https://doi.org/10.1016/j.sse.2019.03.020.
Smalc-Koziorowska, J. *et al.* (2015) 'Elimination of trench defects and V-pits from InGaN/GaN structures', *Applied Physics Letters*, Vol. 106 No. 10. doi: 10.1063/1.4914940.
Son, K. S. *et al.* (2004) 'Formation of V-shaped pits in GaN thin films grown on high temperature GaN', *Journal of Crystal Growth*, Vol. 261 No. 1, pp. 50–54. doi: 10.1016/j.jcrysgro.2003.08.075.
Surender, S. *et al.* (2017) 'Effect of growth temperature on InGaN/GaN heterostructures grown by MOCVD', *Journal of Crystal Growth*, Vol. 468 No. November 2016, pp. 249–251. doi: 10.1016/j.jcrysgro.2016.11.061.
Tao, T. *et al.* (2011) 'Surface morphology and composition studies in InGaN/GaN film grown by MOCVD', *Journal of Semiconductors*, Vol. 32 No. 8, pp. 2009–2012. doi: 10.1088/1674-4926/32/8/083002.
Tassev, V. L. and Vangala, S. R. (2019) 'Thick hydride vapor phase heteroepitaxy: A novel approach to growth of nonlinear optical materials', *Crystals*, Vol. 9 No. 8. doi: 10.3390/cryst9080393.
Tsao, J. Y. *et al.* (2018) 'Ultrawide-Bandgap Semiconductors: Research Opportunities and Challenges', *Advanced Electronic Materials*, Vol. 4 No. 1. doi: 10.1002/aelm.201600501.
Valdueza-Felip, S. *et al.* (2017) 'P-i-n InGaN homojunctions (10–40% In) synthesized by plasma-assisted molecular beam epitaxy with extended photoresponse to 600 nm', *Solar Energy Materials and Solar Cells*, Vol. 160, pp. 355–360. doi: 10.1016/j.solmat.2016.10.007.
Walukiewicz, W. *et al.* (2006) 'Structure and electronic properties of InN and In-rich group III-nitride alloys', *Journal of Physics D: Applied Physics*, Vol. 39 No. 5, pp. R83–R99. doi: 10.1088/0022-3727/39/5/R01.
Wang, H. L. *et al.* (2018) 'Suppression of indium-composition fluctuations in InGaN epitaxial layers by periodically-pulsed mixture of N2 and H2 carrier gas', *Chinese Physics B*, Vol. 27 No. 12. doi: 10.1088/1674-1056/27/12/127805.
Wang, X. *et al.* (2016) 'Investigation of phase separation in InGaN alloys by plasmon loss spectroscopy in a TEM', *MRS Advances*, Vol. 1 No. 40, pp. 2749–2756. doi: 10.1557/adv.2016.542.
Wang, X. *et al.* (2018) 'Influence of InGaN layer growth temperature on luminescence properties of InGaN/GaN multiple quantum wells', *Materials Research Express*, Vol. 5 No. 2. doi: 10.1088/2053-1591/aaaef2.
Wolny, P. *et al.* (2018) 'Dependence of indium content in monolayer-thick InGaN quantum wells on growth temperature in InxGa1-xN/In0.02Ga0.98N superlattices', *Journal of Applied Physics*, Vol. 124 No. 6, pp. 0–9. doi: 10.1063/1.5032287.
Yam, F. K. and Hassan, Z. (2008) 'InGaN: An overview of the growth kinetics, physical properties and emission mechanisms', *Superlattices and Microstructures*, Vol. 43 No. 1, pp. 1–23. doi: 10.1016/j.spmi.2007.05.001.
Yamamoto, A. *et al.* (2013) 'Metal-organic vapor-phase epitaxial growth of InGaN and InAlN for multi-junction tandem solar

cells', *Materials for Renewable and Sustainable Energy*, Vol. 2 No. 2, p. 10. doi: 10.1007/s40243-013-0010-5.
Yusof, A. S. *et al.* (2021) 'The dependence of indium incorporation on specified temperatures in growing InGaN/GaN heterostructure using MOCVD technique', *Materials Research Bulletin*, Vol. 137 No. July 2020. doi: 10.1016/j.materresbull.2020.111176.
Yusof, A. S., Hassan, Z. and Zainal, N. (2018) 'Fabrication and characterization of copper doped zinc oxide by using Co-sputtering technique', *Materials Research Bulletin*, Vol. 97 No. September 2017, pp. 314–318. doi: 10.1016/j.materresbull.2017.09.031.
Zeng, S. W. *et al.* (2009) 'Substantial photo-response of InGaN p-i-n homojunction solar cells', *Semiconductor Science and Technology*, Vol. 24 No. 5. doi: 10.1088/0268-1242/24/5/055009.

Figure 1 Schematic representation of InGaN/GaN heterostructures

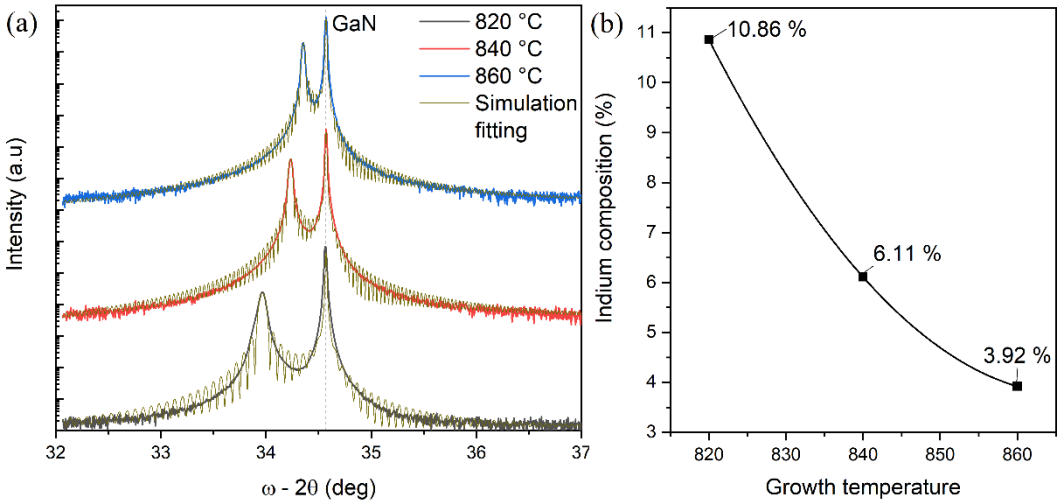

Figure 2 (a) XRD ω-2θ curve pattern of InGaN/GaN heterostructures as a function of different InGaN growth temperatures and (b) indium composition estimated from simulation fitting

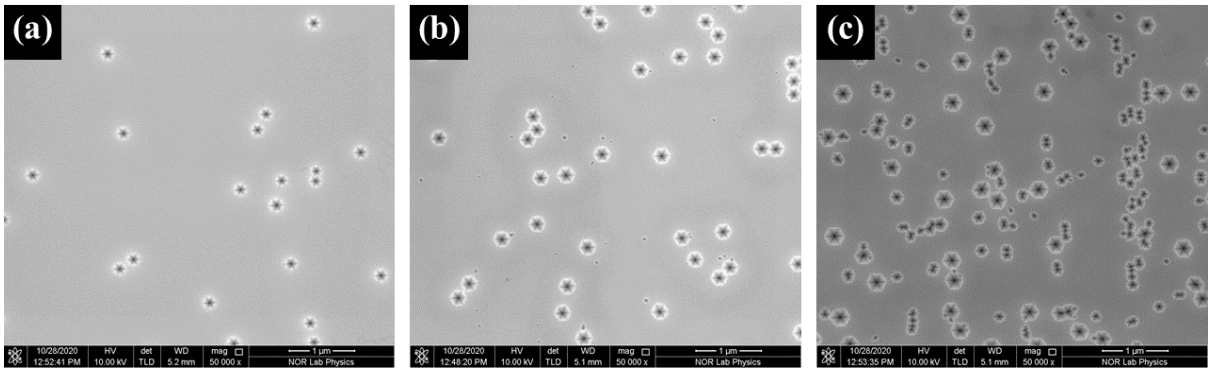

Figure 3 FE-SEM images of InGaN/GaN heterostructure with InGaN layers grown at different temperature (a) 860 °C, (b) 840 °C, (c) 820 °C

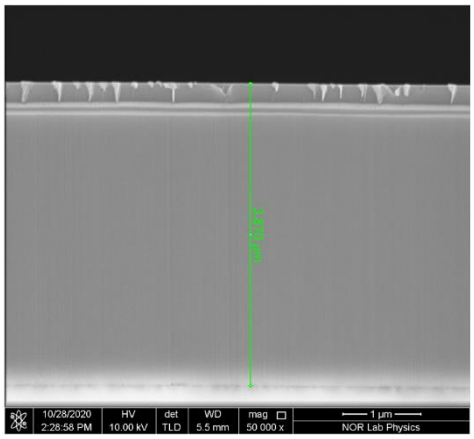

Figure 4 Cross-section view of InGaN/GaN heterostructure with InGaN layer grown at 860 °C

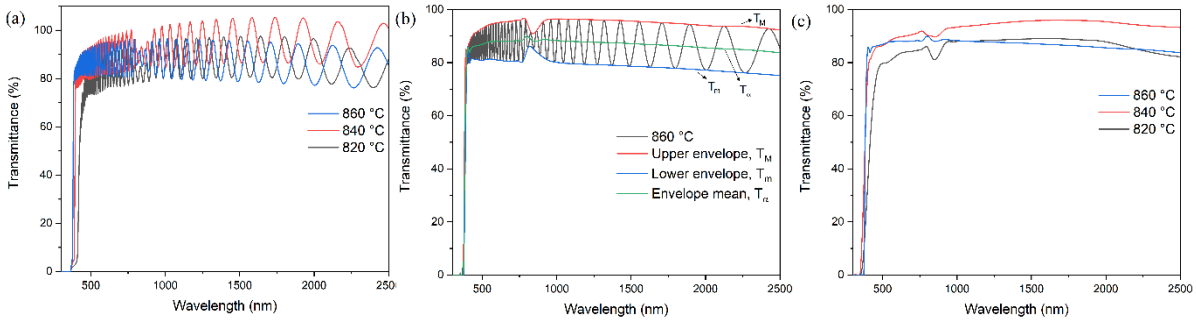

Figure 5 (a) Transmittance spectra of InGaN/GaN heterostructures, (b) transmittance spectra with upper and lower tangent envelope and (c) transmittance geometric mean

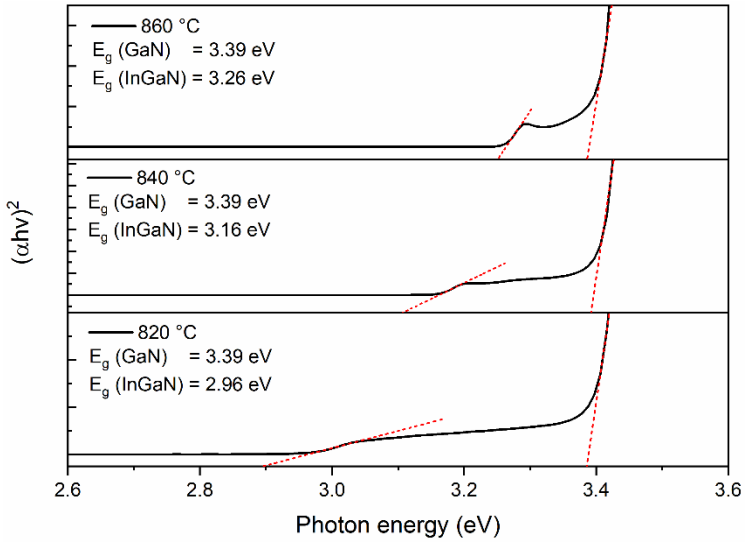

Figure 6 Tauc plot and the optical band gap of the InGaN/GaN heterostructures as a function of InGaN growth temperature

Table I InGaN growth conditions

Parameters	Conditions
Growth temperature	(860, 840, 820) °C
Growth pressure	100 Torr
Growth time	252.6 min
V/III ratio	15177
TMIn/III ratio, TMIn/(TMIn+TEGa)	57.2%

Table II InGaN/GaN structural parameters determined using simulation fitting of XRD diffraction peaks

InGaN growth temperature (°C)	In composition (%)	InGaN thickness (nm)
860	3.92	130
840	6.11	236
820	10.86	258

Table III Calculated indium composition from transmittance spectra using Vegard's Law

Growth temperature (°C)	In composition (%)
860	3.21
840	5.74
820	10.92

Table IV Summary of overall InGaN/GaN heterostructures thickness calculated from the transmittance spectra

InGaN growth temperature (°C)	Thickness	
	Mean, $\bar{d}$ (nm)	Standard deviation, σ (%)
860	3829	0.72
840	3949	0.25
820	4062	0.57

Table V Summary of indium composition and overall thickness estimated using XRD, FE-SEM and UV-Vis spectrometer measurement

InGaN growth temperature (°C)	Indium composition (%)		Overall thickness (nm)		
	XRD	UV-Vis	XRD (InGaN)	FE-SEM	UV-Vis
860	3.92	3.21	130	3870	3829
840	6.11	5.74	236	-	3849
820	10.86	10.92	258	-	4062